Supplement of Clim. Past, 17, 171–201, 2021
https://doi.org/10.5194/cp-17-171-2021-supplement

Climate of the Past
Open Access
EGU

Supplement of

Sequential changes in ocean circulation and biological export productivity during the last glacial–interglacial cycle: a model–data study

Cameron M. O'Neill et al.

Correspondence to: Cameron M. O'Neill (cameron.oneill@anu.edu.au)

1 Additional model parameters described in main text

Table S1. Carbon fluxes and δ^{13}C fractionation signatures of various processes in the SCP-M model

Parameter	**Units**	**Value**	**Reference**
Terrestrial biosphere δ^{13}C	‰	-23	Menviel et al. (2016), Jeltsch-Thommes et al. (2019)
Marine biological productivity δ^{13}C	‰	-19	Schmittner et al. (2013), Hansman and Sessions (2016), Jeltsch-Thommes et al. (2019)
Carbonate weathering DIC flux δ^{13}C	‰	0	Mook (1986)
Volcanic CO_2 δ^{13}C	‰	-4.5	Zeebe (2012)
Marine carbonate δ^{13}C	‰	0	Mook (1986), Sano and Williams (1996)
Air-sea and sea-air δ^{13}C fractionation	Fraction	0.9989-0.999	Mook et al. (1974)
Air-sea and sea-air Δ^{14}C fractionation	Fraction	0.98-0.998	Toggweiler and Sarmiento (1985)
Volcanic CO_2 emissions	mol (GtC) yr^{-1}	6 x 10^{12} (0.1)	Zeebe (2012)
Carbonate weathering flux of C	mol m^{-3} yr^{-1}	1.5	Toggweiler (2008), (Zeebe, 2012)
Silicate base weathering flux of C	mol m^{-3} yr^{-1}	7.5 x 10^{-3}	Toggweiler (2008)
Silicate weathering slope	m^{-3} yr^{-1}	0.7	Toggweiler (2008)
Carbonate weathering C (@275 ppm CO_2)	Tmol yr^{-1}	10	Toggweiler (2008), Zeebe (2012)
Carbonate weather C (@190 ppm CO_2)	Tmol yr^{-1}	7	Toggweiler (2008), Zeebe (2012)
Silicate weather C (@275 ppm CO_2)	Tmol yr^{-1}	6	Toggweiler (2008), Zeebe (2012)
Silicate weather C (@190 ppm CO_2)	Tmol yr^{-1}	5	Toggweiler (2008), Zeebe (2012)
Terrestrial NPP interglacial base rate	PgC yr^{-1}	66	Hoogakker et al. (2016)

2 Model-data experiment forcings

Table S2 shows the sea surface temperature (SST) forcings applied to the SCP-M surface boxes in each MIS, for the purposes of undertaking the model-data experiments as described in the main text.

Table S2. Sea surface temperature (SST) forcings in each MIS and model box from values in Kohfeld and Chase (2017). All values are degrees Celsius relative to modern day GLODAP data. Key to boxes: Atlantic (box 1: low latitude/tropical surface ocean; box 2: northern surface ocean; box 7: subpolar southern surface ocean). Pacific-Indian (box 8: low latitude/tropical surface ocean; box 11: subpolar southern surface ocean). Southern Ocean (box 12: surface ocean).

MIS	**Time (ka)**	**Box 1 (±°C)**	**Box 2 (±°C)**	**Box 7 (±°C)**	**Box 8 (±°C)**	**Box 11 (±°C)**	**Box 12 (±°C)**
∼1	0-11.7	1.09	0.66	1.62	1.01	1.62	1.71
∼2	18-29	-1.45	-6.45	-1.42	-2.49	-1.42	-0.74
3	29-57	-1.96	-5.17	-1.82	-2.63	-1.82	-1.27
4	57-71	-1.7	-5.77	-1.61	-2.54	-1.61	-0.8
5a	79.5-84.5	-0.27	-2.25	-0.22	-0.63	-0.22	0.53
5b	84.5-89.5	-0.56	-2.89	-0.56	-1.02	-0.56	-0.14
5c	91-101	0.02	-2.2	-0.43	-0.41	-0.43	-0.2
5d	104-114	-0.07	-1.62	-0.49	-0.4	-0.49	-0.1
5e	118-128	0.95	1.25	0.94	1.05	0.94	0.87

Table S3 shows forcings for other environmental parameters applied in the model-data experiments described in the main text.

Table S3. Model forcings for MIS across the last glacial-interglacial cycle. Proxy for Antarctic sea ice extent using ssNa fluxes from the EPICA Dome C ice core (Wolff et al., 2010), used to temporally contour MIS model forcings for salinity (Adkins et al., 2002) and polar Southern Ocean piston velocity. Global ocean salinity is forced to a glacial maximum of +1 psu and the polar Southern Ocean is forced to +2 psu, as modified from Adkins et al. (2002). Ocean volume forced using global relative sea level reconstruction of Rohling et al. (2009). Atmospheric ^{14}C production rate time series for 0-50 ka of Muscheler et al. (2014). Long-term values assumed for >50 ka (Key, 2001). Reef carbonate flux of carbon from Ridgwell et al. (2003) profiled across the glacial cycle using a curve from Opdyke and Walker (1992).

MIS	Southern Ocean (box 12) piston velocity (m day^{-1})	Ocean volume (% of modern)	Coral reef C flux (x 10^{12} mol C annum^{-1})	^{14}C production (atoms s^{-1})	Salinity ($\pm$ psu)	
					Southern Ocean (box 12)	**Rest of ocean**
$\sim$1	3.92	99.9%	4.3	1.64	0.59	0.3
$\sim$2	2.63	97.5%	-1.6	2.39	1.94	0.97
3	2.76	98%	-0.5	2.28	1.99	0.99
4	2.84	97.9%	0.9	1.84	1.85	0.93
5a	3.06	99.1%	2.1	1.75	1.47	0.73
5b	2.77	98.4%	2.4	1.75	1.71	0.86
5c	3.14	98.9%	3	1.75	0.98	0.49
5d	2.88	99.1%	3.8	1.75	1.32	0.66
5e	4.17	99.8%	4.8	1.75	-0.03	-0.01

3 Data compilation

Table S4 shows atmospheric proxy data averaged into MIS slices.

Table S4. Data for atmospheric CO_2 (Monnin et al., 2004; MacFarling Meure et al., 2006; Bereiter et al., 2012; Rubino et al., 2013; Schneider et al., 2013; Ahn and Brook, 2014; Marcott et al., 2014; Bereiter et al., 2015), atmospheric $\delta^{13}C$ (Elsig et al., 2009; Schmitt et al., 2012; Schneider et al., 2013; Eggleston et al., 2016) and atmospheric $\Delta^{14}C$ (Reimer et al., 2009), averaged into MIS time slices. nan = "not a number" due to no data.

MIS	**CO_2 (ppm)**	**$\delta^{13}C$ (‰)**	**$\Delta^{14}C$ (‰)**
∼1	272.2±7.8	-6.41±0.09	57.1±47.9
∼2	189.1±3.1	-6.42±0.03	466±80
3	202.6±8.6	-6.55±0.14	517.8±131.5
4	210±9.6	-6.63±0.2	nan
5a	239.2±7	-6.47±0.01	nan
5b	226.6±6.6	-6.47±0.01	nan
5c	240.7±5.3	-6.6±0.08	nan
5d	249.2±9	-6.68±0.03	nan
5e	275.9±3.3	-6.66±0.08	nan

Tables S5-S7 shows ocean $\delta^{13}C$, CO_3^{2-} and $\Delta^{14}C$ proxy data mapped and averaged into SCP-M boxes, and averaged in MIS slices.

Table S5. Ocean $\delta^{13}C$ data (‰) sourced from Oliver et al. (2010), Govin et al. (2009) and Piotrowski et al. (2009) mapped into SCP-M boxes and averaged for each MIS. Data are sourced from *Cibicides* species, hence incomplete coverage of the ocean boxes. Key to boxes: Atlantic (box 1: low latitude/tropical surface ocean; box 2: northern surface ocean; box 3: intermediate ocean; box 4: deep ocean; box 6: abyssal ocean; box 7: subpolar southern surface ocean). Pacific-Indian (box 8: low latitude/tropical surface ocean; box 9: deep ocean; box 10: abyssal ocean; box 11: subpolar southern surface ocean). Southern Ocean (box 5: intermediate-deep; box 12: surface ocean). nan = "not a number" due to no data.

MIS	**Box 1**	**Box 2**	**Box 3**	**Box 4**	**Box 5**	**Box 6**	**Box 7**	**Box 8**	**Box 9**	**Box 10**	**Box 11**	**Box 12**
∼1	nan	nan	0.93±0.5	0.95±0.3	nan	0.73±0.4	nan	nan	0.57±0.4	0.12±0.2	nan	nan
∼2	nan	nan	1.46±0.4	0.99±0.4	nan	0.12±0.5	nan	nan	0.2±0.2	-0.37±0.3	nan	nan
3	nan	nan	1.4±0.2	0.95±0.4	nan	0.33±0.9	nan	nan	0.4±0.3	-0.22±0.3	nan	nan
4	nan	nan	1.31±0.3	0.9±0.4	nan	0.18±0.6	nan	nan	0.25±0.3	-0.54±0.3	nan	nan
5a	nan	nan	nan	0.92±0.3	nan	0.54±0.5	nan	nan	0.66±0.5	-0.23±0.3	nan	nan
5b	nan	nan	nan	0.87±0.3	nan	0.48±0.5	nan	nan	0.55±0.4	-0.15±0.2	nan	nan
5c	nan	nan	nan	0.95±0.3	nan	0.66±0.4	nan	nan	0.58±0.5	-0.13±0.3	nan	nan
5d	nan	nan	nan	0.84±0.3	nan	0.46±0.4	nan	nan	0.47±0.5	-0.33±0.3	nan	nan
5e	nan	nan	nan	0.7±0.3	nan	0.48±0.4	nan	nan	0.36±0.3	-0.02±0.3	nan	nan

Table S6. Ocean CO_3^{2-} data (μmol kg^{-1}), mapped into SCP-M boxes and averaged for each MIS. Key to boxes: Atlantic (box 1: low latitude/tropical surface ocean; box 2: northern surface ocean; box 3: intermediate ocean; box 4: deep ocean; box 6: abyssal ocean; box 7: subpolar southern surface ocean). Pacific-Indian (box 8: low latitude/tropical surface ocean; box 9: deep ocean; box 10: abyssal ocean; box 11: subpolar southern surface ocean). Southern Ocean (box 5: intermediate-deep; box 12: surface ocean). nan = "not a number" due to no data.

MIS	Box 1	Box 2	Box 3	Box 4	Box 5	Box 6	Box 7	Box 8	Box 9	Box 10	Box 11	Box 12
∼1	292.1±9	178.7±10	nan	116.6±5	nan	106.8±12	nan	nan	73.5±4	85.1±9	nan	nan
∼2	335±18	215.3±4	nan	141.7±3	nan	91±17	nan	nan	75.9±5	83.5±9	nan	nan
3	286.9±nan	nan	nan	135.6±6	nan	107.7±18	nan	nan	72.5±3	84.9±12	nan	nan
4	nan	nan	nan	nan	nan	82.7±16	nan	nan	66.3±4	70.9±14	nan	nan
5a	nan	nan	nan	nan	nan	104.6±11	nan	nan	71.9±8	nan	nan	nan
5b	nan	nan	nan	nan	nan	94.9±17	nan	nan	71.5±9	72.9±13	nan	nan
5c	nan	nan	nan	nan	nan	108.2±13	nan	nan	72.5±5	73.6±8	nan	nan
5d	nan	nan	nan	nan	nan	112±10	nan	nan	63.1±6	66.5±12	nan	nan
5e	nan	nan	nan	nan	nan	115.7±9	nan	nan	67.7±6	72.6±4	nan	nan

Data sourced from Yu et al. (2010), Yu et al. (2013), Yu et al. (2014b), Yu et al. (2014a), Broecker et al. (2015), Yu et al. (2016), Qin et al. (2017), Qin et al. (2018), Chalk et al. (2019).

Table S7. Ocean $\Delta^{14}C$ data (‰), mapped into SCP-M boxes and averaged for each MIS. Key to boxes: Atlantic (box 1: low latitude/tropical surface ocean; box 2: northern surface ocean; box 3: intermediate ocean; box 4: deep ocean; box 6: abyssal ocean; box 7: subpolar southern surface ocean). Pacific-Indian (box 8: low latitude/tropical surface ocean; box 9: deep ocean; box 10: abyssal ocean; box 11: subpolar southern surface ocean). Southern Ocean (box 5: intermediate-deep; box 12: surface ocean). nan = "not a number" due to no data.

MIS	Box 1	Box 2	Box 3	Box 4	Box 5	Box 6	Box 7	Box 8	Box 9	Box 10	Box 11	Box 12
∼1	16.9±47	48.6±40	-66.9±109	27.7±99	nan	-31±124	-63.1±77	7.1±47	-80.4±76	-101.5±65	-6.6±58	nan
∼2	332.5±86	312.4±131	315.7±199	236.5±130	nan	73±202	243.4±151	320.6±146	153±176	67.2±174	315.8±116	nan
3	nan	nan	nan	nan	nan	236.8±93	499.1±36	413.1±112	404.8±123	-46.3±202	297.4±244	nan
4	nan	nan	nan	nan	nan	nan	nan	nan	nan	nan	nan	nan
5a	nan	nan	nan	nan	nan	nan	nan	nan	nan	nan	nan	nan
5b	nan	nan	nan	nan	nan	nan	nan	nan	nan	nan	nan	nan
5c	nan	nan	nan	nan	nan	nan	nan	nan	nan	nan	nan	nan
5d	nan	nan	nan	nan	nan	nan	nan	nan	nan	nan	nan	nan
5e	nan	nan	nan	nan	nan	nan	nan	nan	nan	nan	nan	nan

Data sourced from Skinner and Shackleton (2004), Marchitto et al. (2007), Barker et al. (2010), Bryan et al. (2010), Skinner et al. (2010), Burke and Robinson (2012), Davies-Walczak et al. (2014), Skinner et al. (2015), Chen et al. (2015), Hines et al. (2015), Sikes et al. (2016), Ronge et al. (2016), Skinner et al. (2017), Zhao et al. (2017).

3.1 Statistical analysis of ocean δ^{13}C data

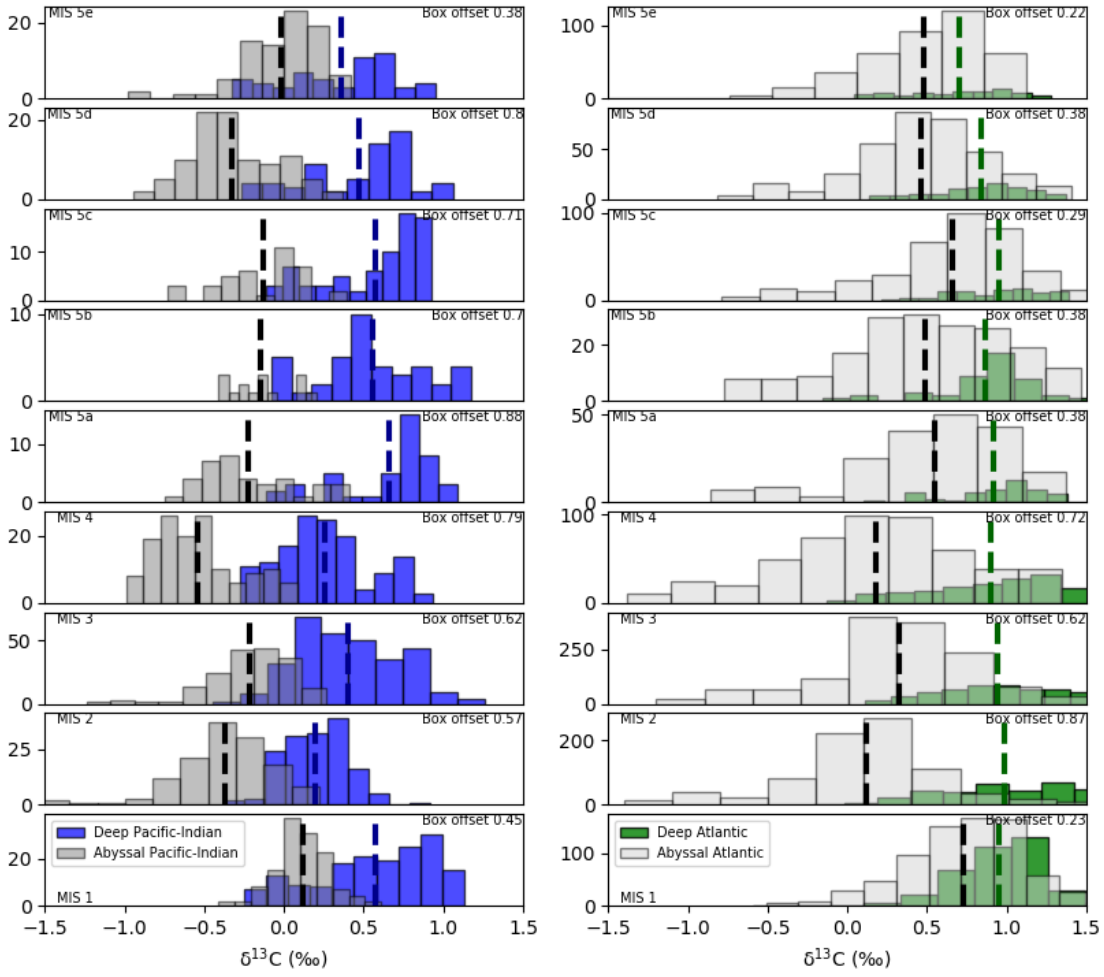

Figure S1. Distribution histograms of δ^{13}C data for the Pacific-Indian (left column) and Atlantic Ocean (right column) deep (100/1,000-2,500m) and abyssal (>2,500m) boxes, for each MIS. Mean δ^{13}C in each box shown by the vertical dashed lines. Deep-abyssal offsets in mean δ^{13}C shown in the top right-hand corner of each panel.

Table S8. Welch's paired T-tests for the independence of deep-abyssal offsets in mean δ^{13}C with respect of the penultimate interglacial period (MIS 5e), for the periods MIS 1-5e. The null hypothesis is that the deep-abyssal offset in mean δ^{13}C in each MIS is not statistically independent of MIS 5e (i.e. statistically the same and not supportive of a change in deep-abyssal δ^{13}C distribution that may be delivered by a changed ocean process). p-values>0.05 lead to the null hypothesis being accepted, whereas p-values <0.05 lead to the null hypothesis being rejected and confirm statistical independence of the deep-abyssal offsets relative to MIS 5e (perhaps supportive of a changed ocean distributive process in the glacial period). Deep-abyssal offsets for the Pacific-Indian during MIS 2-MIS 5d are statistically independent of MIS 5e, supportive of a changed oceanic distribution of δ^{13}C throughout the glacial period. The MIS 1 Pacific-Indian deep-abyssal δ^{13}C offset is not statistically independent of MIS 5e, indicating a similar deep-abyssal δ^{13}C distribution between the last and penultimate interglacial periods. For the Atlantic Ocean, deep-abyssal mean δ^{13}C offsets are not statistically independent with respect to MIS 5e (p-value >0.05, accept null hypothesis), until the period MIS 2-4. Atlantic deep-abyssal mean δ^{13}C offset in MIS 1 is not statistically different from MIS 5e.

	Pacific-Indian (vs MIS 5e)			Atlantic (vs MIS 5e)		
MIS	t-statistic	p-value	Accept/ reject null	t-statistic	p-value	Accept/ reject null
MIS 5e	0.0	0.500	Accept	0.0	0.500	Accept
MIS5d	3.8	0.000	Reject	1.4	0.079	Accept
MIS5c	3.0	0.002	Reject	0.7	0.253	Accept
MIS5b	2.9	0.002	Reject	1.5	0.074	Accept
MIS5a	4.5	0.000	Reject	1.4	0.082	Accept
MIS4	3.7	0.000	Reject	4.5	0.000	Reject
MIS3	2.1	0.017	Reject	3.6	0.000	Reject
MIS2	1.7	0.044	Reject	5.9	0.000	Reject
MIS1	0.7	0.246	Accept	0.1	0.478	Accept

4 Model-data experiment results

Table S9 shows the parameter values for global overturning circulation (GOC, Psi_1), Atlantic meridional overturning circulation (AMOC, Psi_2) and Southern Ocean biological export productivity (Z) from the model-data experiments described in the main text.

Table S10 shows the optimised model-data experiment results for atmospheric CO_2, δ^{13}C and Δ^{14}C, and the terrestrial biosphere.

Table S11 shows the optimised model-data experiment results for oceanic δ^{13}C.

Table S12 shows the optimised model-data experiment results for oceanic CO_3^{2-}.

Table S9. Model-data experiment optimised values for ocean parameters in each MIS.

MIS	Psi_1 **(Sv)**	Psi_2 **(Sv)**	**Atlantic (Pacific-Indian) Southern Ocean** Z **(mol C m^{-2} yr^{-1}**
∼1	29	18	3.4 (2.4)
∼2	16	13	4.7 (3.3)
3	16	13	2.6 (1.8)
4	18	13	3.9 (2.8)
5a	20	15	2.4 (1.7)
5b	19	14	3 (2.1)
5c	22	16	2.8 (2)
5d	22	16	2.8 (2)
5e	29	18	3.2 (2.2)

Table S10. Model-data experiment model results for atmospheric CO_2, atmospheric δ^{13}C, atmospheric Δ^{14}C, terrestrial biosphere net primary productivity (NPP) and carbon stock in each MIS.

MIS	**CO_2 (ppm)**	δ^{13}**C (‰)**	Δ^{14}**C (‰)**	**Terrestrial biosphere NPP (PgC a^{-1})**	**Terrestrial biosphere carbon stock (PgC)**
∼1	270.8	-6.39	48.6	73.1	2368.1
∼2	188.7	-6.43	526.2	51.4	1767.8
3	203.6	-6.57	479.9	56.3	1936.8
4	208.8	-6.61	212.4	55.4	1794.1
5a	241.2	-6.47	139.1	60.9	2094
5b	228	-6.48	153.1	63.3	2051.7
5c	241.7	-6.59	131.5	63.9	2070.3
5d	248.2	-6.68	122	58.8	1903.9
5e	275.1	-6.65	96.5	66.4	2152.2

Table S13 shows the optimised model-data experiment results for oceanic Δ^{14}C.

Table S11. Model-data experiment model results for ocean $\delta^{13}C$ (‰) in each MIS. Key to boxes: Atlantic (box 1: low latitude/tropical surface ocean; box 2: northern surface ocean; box 3: intermediate ocean; box 4: deep ocean; box 6: abyssal ocean; box 7: subpolar southern surface ocean). Pacific-Indian (box 8: low latitude/tropical surface ocean; box 9: deep ocean; box 10: abyssal ocean; box 11: subpolar southern surface ocean). Southern Ocean (box 5: intermediate-deep; box 12: surface ocean).

MIS	Box 1	Box 2	Box 3	Box 4	Box 5	Box 6	Box 7	Box 8	Box 9	Box 10	Box 11	Box 12
∼1	2.65	2.57	1.94	1.13	0.67	0.72	2	3.11	0.39	0.23	2.65	2.04
∼2	3.11	3.01	2.26	0.95	0.26	0.01	2.29	3.34	0.03	-0.48	3.35	1.8
3	2.94	2.89	2.13	1.12	0.36	0.19	2.19	3.29	0.13	-0.33	2.99	1.82
4	2.89	2.84	2.08	0.9	0.29	0.05	2.16	3.17	0.05	-0.36	3.01	1.8
5a	2.8	2.75	2.04	1.16	0.45	0.52	2.12	3.18	0.21	-0.11	2.8	1.9
5b	2.9	2.86	2.11	1.11	0.44	0.38	2.21	3.24	0.2	-0.17	2.95	1.93
5c	2.67	2.59	1.93	1.08	0.44	0.53	1.99	3.07	0.19	-0.08	2.7	1.85
5d	2.56	2.49	1.83	0.99	0.34	0.44	1.9	2.94	0.09	-0.18	2.61	1.73
5e	2.42	2.36	1.74	0.98	0.54	0.59	1.81	2.89	0.27	0.12	2.47	1.92

Table S12. Model-data experiment model results for ocean CO_3^{2-} (μmol kg^{-1}) in each MIS. Key to boxes: Atlantic (box 1: low latitude/tropical surface ocean; box 2: northern surface ocean; box 3: intermediate ocean; box 4: deep ocean; box 6: abyssal ocean; box 7: subpolar southern surface ocean). Pacific-Indian (box 8: low latitude/tropical surface ocean; box 9: deep ocean; box 10: abyssal ocean; box 11: subpolar southern surface ocean). Southern Ocean (box 5: intermediate-deep; box 12: surface ocean).

MIS	Box 1	Box 2	Box 3	Box 4	Box 5	Box 6	Box 7	Box 8	Box 9	Box 10	Box 11	Box 12
∼1	271.5	206.8	192.8	121.5	79.7	102.8	161.3	258.3	70.7	76.3	174.6	137.5
∼2	330.2	236.1	242.1	123.6	84.1	96.5	196.4	301.7	75.6	76.2	212.2	157.5
3	314.6	230.2	228.7	132.8	83	103.7	185.9	289.4	75.1	76.3	199	151
4	307.9	219.8	222.3	114.2	80.6	92.1	180.1	285.5	72.2	76.2	197.7	150.3
5a	284.2	210.2	202.2	121.3	78.5	95.6	165.6	271.6	70.4	76.3	183.1	142.2
5b	286.5	210.7	204.3	114.4	77.1	87.9	166.4	273.9	69.3	76.2	185.8	141.6
5c	291.2	215.4	207.6	128.5	80.4	106.8	169.6	273.2	72.2	76.3	182.5	141.1
5d	289.7	216.8	206.6	129	79.7	106.6	168.8	272.4	71.6	76.3	181.4	140.1
5e	271.8	209.8	191.9	123.8	79.5	104	159.5	259.8	70.8	76.3	171.7	135

Table S13. Model-data experiment model results for ocean $\Delta^{14}C$ (‰) in each MIS. Key to boxes: Atlantic (box 1: low latitude/tropical surface ocean; box 2: northern surface ocean; box 3: intermediate ocean; box 4: deep ocean; box 6: abyssal ocean; box 7: subpolar southern surface ocean). Pacific-Indian (box 8: low latitude/tropical surface ocean; box 9: deep ocean; box 10: abyssal ocean; box 11: subpolar southern surface ocean). Southern Ocean (box 5: intermediate-deep; box 12: surface ocean).

MIS	**Box 1**	**Box 2**	**Box 3**	**Box 4**	**Box 5**	**Box 6**	**Box 7**	**Box 8**	**Box 9**	**Box 10**	**Box 11**	**Box 12**
∼1	-18.1	-22	-42.2	-77.8	-80.7	-102.8	-53.6	-34	-88.3	-138.6	-12.1	-37.7
∼2	386.2	389.8	328.6	240.4	207.1	127.8	303.8	357.4	195.3	55.8	424.4	292.1
3	357.2	358.8	302.2	219.9	190.8	112.2	278.7	333.5	179.4	43	383.2	272.9
4	117.7	119.8	80.9	20.5	6.3	-52.5	63	91.1	-2.1	-96.7	136.9	64.6
5a	60.5	58.8	29.3	-20	-32.6	-67.9	14.6	37.8	-40.5	-121.3	73.8	20.2
5b	71.1	70.6	38.5	-14.7	-27.1	-71	22.7	46.1	-35.1	-120.6	86	27.1
5c	51.5	49.1	21.8	-23.8	-34.5	-63.9	8	31.7	-42.6	-115.2	64.3	16.9
5d	44.3	41.5	15	-30.5	-41.7	-70.5	1.3	23.6	-49.6	-121.5	56.7	8
5e	27.2	22.6	0.3	-38.7	-41.5	-65.4	-11.7	13.1	-50.2	-103.7	33.6	6.7

Figure S2 shows the full range of experiments undertaken and the resulting model-data error mesh charts. These charts plot the difference between the model outputs and the proxy data, as a function of each of the three parameters varied in the model-data experiments (Psi_1, Psi_2 and Z).

5 Model code and data

The model code, processed data files, model-data experiment results, and any (published) raw proxy data gathered in the course of this work, are located at https://doi.org/10.5281/zenodo.3559339. No original data was created, or unpublished data used, in this work. Figure S3 provides an overview of the files contained in the Zenodo repository, and their linkages. For more detail on the SCP-M equations, see O'Neill et al. (2019).

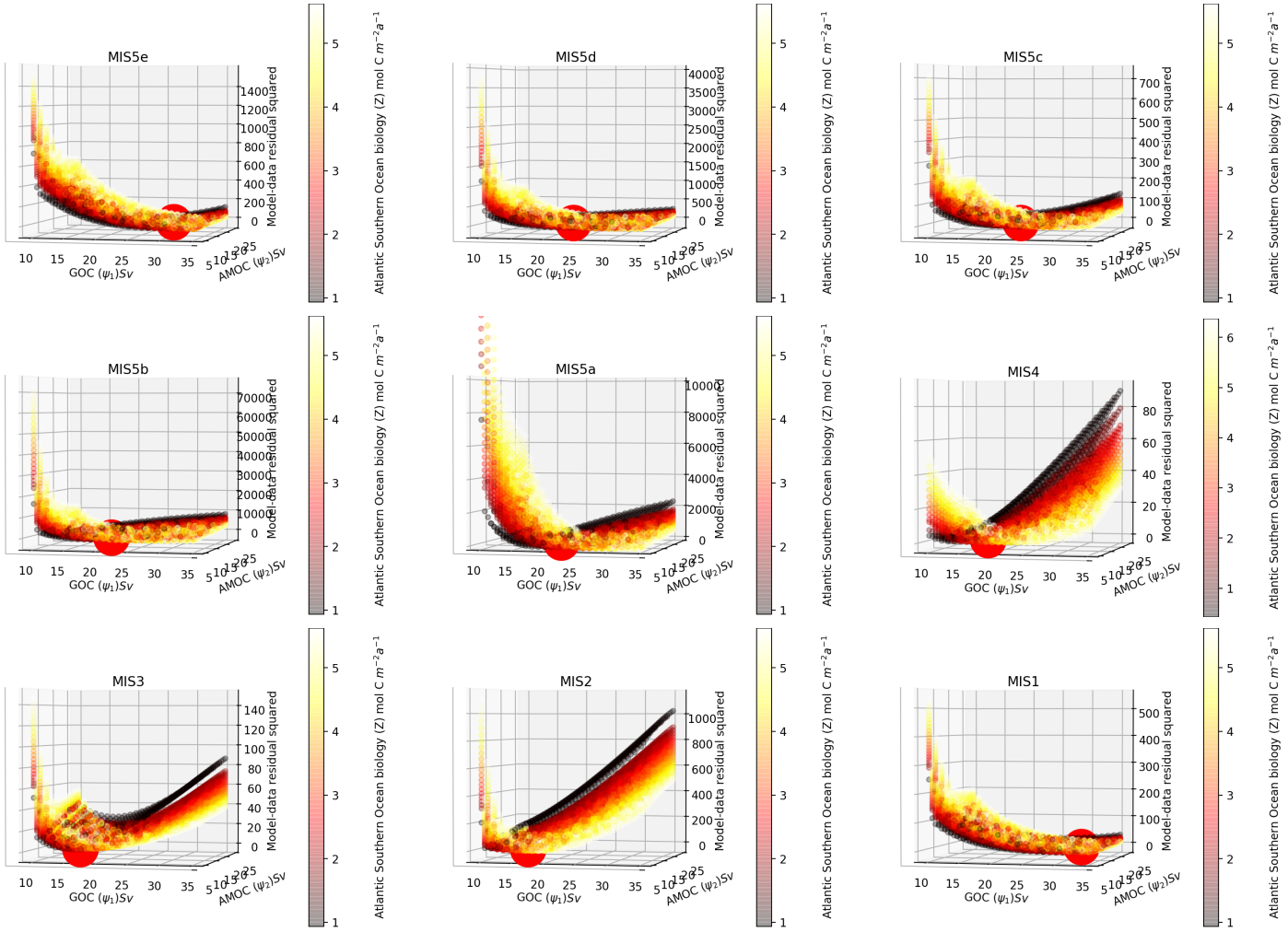

Figure S2. Model-data error surfaces for each of the model-data experiments within each MIS. The figures show the variation in the model-data residual, the "error" (the square of model results less data points) across the parameter input ranges for global overturning circulation (Ψ_1), Atlantic meridional overturning circulation (Ψ_2) and Atlantic Southern Ocean biological export productivity (Z). The latter (Z) is shown as the variations in colour of the data points, with the scale shown on the colour bar. The optimised values for the parameters are found at the bottom turning point of the curves, at the minimum of the model-data residual. The model-data residual is most sensitive to variations in Ψ_1 along the x-axis, which shows increases in the model-data residual with variations in Ψ_1 above and below the optimised value at the minimum residual

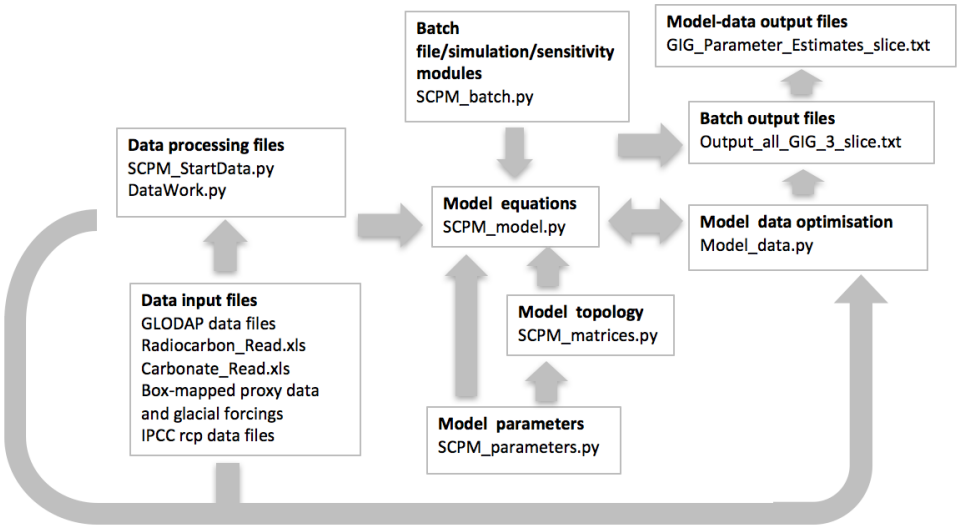

Figure S3. SCP-M files contained in the Zenodo repository at https://doi.org/10.5281/zenodo.4430066. The repository contains the model code and processed data files. Raw (published) data for carbonate ion proxy and $\Delta^{14}C$ gathered as part of the work is contained in spreadsheets in the data inputs folder. No new data was created, or unpublished data used, in this work.

References

Adkins, J., McIntyre, K., and Schrag, D.: The Salinity, Temperature, and $\delta^{18}O$ of the Glacial Deep Ocean, Science, 298, 1769–1773, 2002.

Ahn, J. and Brook, E.: Siple Dome ice reveals two modes of millennial CO_2 change during the last ice age, Nature Communications, 5:3723, doi: 10.1038/ ncomms4723, 2014.

Barker, S., Knorr, G., Vautravers, M., Diz, P., and Skinner, L.: Extreme deepening of the Atlantic overturning circulation during deglaciation, Nature Geoscience, 3, 567–571, 2010.

Bereiter, B., Lüthi, D., Siegrist, M., Schüpbach, S., Stocker, T. F., and Fischer, H.: Mode change of millennial CO_2 variability during the last glacial cycle associated with a bipolar marine carbon seesaw, Proc. Natl. Acad. Sci. U.S.A., 109, 9755–9760, 2012.

Bereiter, B., Eggleston, S., Schmitt, J., Nehrbass-Ahles, C., Stocker, T., Fischer, H., Kipfstuhl, S., and Chappellaz, J.: Revision of the EPICA Dome C CO_2 record from 800 to 600kyr before present, Geophys. Res. Lett, 42, 542–549, 2015.

Broecker, W., Yu, J., and Putnam, A.: Two contributors to the glacial CO_2 decline, Earth and Planetary Science Letters, 429, 191–196, 2015.

Bryan, S., Marchitto, T., and Lehman, S.: The release of ^{14}C-depleted carbon from the deep ocean during the last deglaciation: Evidence from the Arabian Sea, Earth and Planetary Science Letters, 298, 244–254, 2010.

Burke, A. and Robinson, L.: The Southern Ocean's Role in Carbon Exchange During the Last Deglaciation, Science, 335, 557–561, 2012.

Chalk, T., Foster, G., and Wilson, P.: Dynamic storage of glacial CO_2 in the Atlantic Ocean revealed by boron $[CO_3^{2-}]$ and pH records, Earth and Planetary Science Letters, 510, 1–11, 2019.

Chen, T., Robinson, L., Burke, A., Southon, J., Spooner, P., Morris, P., and Ng, H.: Synchronous centennial abrupt events in the ocean and atmosphere during the last deglaciation, Science, 349, 1537–1541, 2015.

Davies-Walczak, M., Mix, A., Stoner, J., Southon, J., Cheseby, M., and Xuan, C.: Late Glacial to Holocene radiocarbon constraints on North Pacific Intermediate Water ventilation and deglacial atmospheric CO_2 sources, Earth and Planetary Science Letters, 397, 57–66, 2014.

Eggleston, S., Schmitt, J., Bereiter, B., Schneider, R., and Fischer, H.: Evolution of the stable carbon isotope composition of atmospheric CO_2 over the last glacial cycle, Paleoceanography, 31, 434–452, 2016.

Elsig, J., Schmitt, J., Leuenberger, D., Schneider, R., Eyer, M., Leuenberger, M., Joos, F., Fischer, H., and Stocker, T. F.: Stable isotope constraints on Holocene carbon cycle changes from an Antarctic ice core,, Nature, 461, 507–510, 2009.

Govin, A., Michel, E., Labeyrie, L., Waelbroeck, C., Dewilde, F., and Jansen, E.: Evidence for northward expansion of Antarctic Bottom Water mass in the Southern Ocean during the last glacial inception, Paleoceanography, 24, doi:10.1029/2008PA001 603, 2009.

Hansman, R. and Sessions, A.: Measuring the in situ carbon isotopic composition of distinct marine plankton populations sorted by flow cytometry, Limnology and Oceanography: methods, 14, 87–99, 2016.

Hines, S., Southon, J., and Adkins, J.: A high-resolution record of Southern Ocean intermediate water radiocarbon over the past 30,000 years, Earth and Planetary Science Letters, 432, 46–48, 2015.

Hoogakker, B. et al.: Terrestrial biosphere changes over the last 120 kyr, Climate of the Past, 12, 51–73, 2016.

Jeltsch-Thommes, A., Battaglia, G., Cartapanis, O., Jaccard, S., and Joos, F. J.: Low terrestrial carbon storage at the Last Glacial Maximum: constraints from multi-proxy data, Climate of the Past, 15, 849–879, 2019.

Key, R.: Ocean process tracers: Radiocarbon. In: Encyclopedia of Ocean Sciences, pp. 2338–2353, Academic Press, London, 2001.

Kohfeld, K. and Chase, Z.: Temporal evolution of mechanisms controlling ocean carbon uptake during the last glacial cycle, Earth and Planetary Science Letters, 472, 206–215, 2017.

MacFarling Meure, C., Etheridge, D., Trudinger, C., Steele, P., Langenfelds, R., van Ommen, T., Smith, A., and Elkins, J.: Law Dome CO_2, CH_4 and N_2O ice core records extended to 2000 years BP, Geophysical Research Letters, 33, L14 810, doi:10.1029/2006GL026 152, 2006.

Marchitto, T., Lehman, S., Ortiz, J., Flückiger, J., and van Geen, A.: Marine Radiocarbon Evidence for the Mechanism of Deglacial Atmospheric CO_2 Rise, Science, 316, 1456–1459, 2007.

Marcott, S., Bauska, T., Buizert, C., Steig, E., Rosen, J., Cuffey, K., Fudge, T. J., Severinghaus, J. P., Ahn, J., Kalk, M. L., McConnell, J. R., Sowers, T., Taylor, K., White, J. W. C., and Brook, E.: Centennial-scale changes in the global carbon cycle during the last deglaciation, Nature, 514, 616–621, 2014.

Menviel, L., Yu, J., Joos, F., Mouchet, A., Meissner, K. J., and England, M. H.: Poorly ventilated deep ocean at the Last Glacial Maximum inferred from carbon isotopes: A data-model comparison study, Paleoceanography, 31, 2–17, 2016.

Monnin, E., Steig, E., Siegenthaler, U., Kawamura, K., Schwander, J., Stauffer, B., Stocker, T., Morse, D., Barnola, J., Bellier, B., Raynaud, D., and Fischer, H.: Evidence for substantial accumulation rate variability in Antarctica during the Holocene, through synchronization of CO_2 in the Taylor Dome, Dome C and DML ice cores, Earth and Planetary Science Letters, 224, 45–54, 2004.

Mook, W.: ^{13}C in atmospheric CO_2, Netherlands Journal of Sea Research, pp. 211–223, 1986.

Mook, W., Bommerson, J., and Staverman, W.: Carbon Isotope Fractionation Between Dissolved Bicarbonate and Gaseous Carbon Dioxide, Earth and Planetary Science Letters, 22, 169–176, 1974.

Muscheler, R., Beer, J., Wagner, G., Laj, C., Kissel, C., Raisbeck, G., Yioud, F., and Kubik, P.: Changes in the carbon cycle during the last deglaciation as indicated by the comparison of ^{10}Be and ^{14}C records, Earth and Planetary Science Letters, 219, 325–340, 2014.

Oliver, K., Hoogakker, B., Crowhurst, S., Henderson, G., Rickaby, R., Edwards, N., and Elderfield, H.: A synthesis of marine sediment core $\delta^{13}C$ data over the last 150,000 years, Climate of the Past, 6, 645–673, 2010.

O'Neill, C., A. Mc. Hogg, M.J. Ellwood, S. E., and Opdyke, B.: The [simple carbon project] model v1.0, Geosci. Model Dev., 12, 1541–1572, https://doi.org/10.5194/gmd–12–1541–2019, 2019.

Opdyke, B. and Walker, J.: Return of the coral reef hypothesis: Basin to shelf partitioning of $CaCO_3$ and its effect on atmospheric CO_2, Geology, 20, 733–736, 1992.

Piotrowski, A., Banakar, V., Scrivner, A., Elderfield, H., Galy, A., and Dennis, A.: Indian Ocean circulation and productivity during the last glacial cycle, Earth and Planetary Science Letters, 285, 179–189, 2009.

Qin, B., Li, T., Xiong, Z., Algeo, T. J., and Chang, F.: Deepwater carbonate ion concentrations in the western tropical Pacific since 250 ka: Evidence for oceanic carbon storage and global climate influence, Paleoceanography, 32, 351–370, 2017.

Qin, B., Li, T., Xiong, Z., Algeo, T., and Jia, Q.: Deep-Water Carbonate Ion Concentrations in the Western Tropical Pacific Since the Mid-Pleistocene: A Major Perturbation During the Mid-Brunhes, Journal of Geophysical Research: Oceans, 123, 6876–6892, https://doi.org/10.1029/2018JC014 084, 2018.

Reimer, P., Baillie, M., Bard, E., Bayliss, A., Beck, J., Blackwell, P., Ramsey, C. B., Buck, C., Burr, G., Edwards, R., Friedrich, M., Grootes, P., Guilderson, T., Hajdas, I., Heaton, T., Hogg, A., Hughen, K., Kaiser, K., Kromer, B., McCormac, F., Manning, S., Reimer, R., Richards, D., Southon, J., Talamo, S., Turney, C., van der Plicht, J., and Weyhenmeyer, C.: IntCal09 and Marine09 radiocarbon age calibration curves, 0-50,000 years cal BP., Radiocarbon, 51, 1111–50, 2009.

Ridgwell, A., Watson, A., Maslin, M., and Kaplan, J.: Implications of coral reef buildup for the controls on atmospheric CO_2 since the Last Glacial Maximum, Paleoceanography, 18, 1083, doi:10.1029/2003PA000 893, 2003.

Rohling, E., Grant, K., Bolshaw, M., Roberts, A., Siddall, M., Hemleben, C., and Kucera, M.: Antarctic temperature and global sea level closely coupled over the past five glacial cycles, Nature Geoscience, 2, 500–504, 2009.

Ronge, T., Tiedemann, R., Lamy, F., Kohler, P., Alloway, B., Pol-Holz, R. D., Pahnke, K., Southon, J., and Wacker, L.: Radiocarbon constraints on the extent and evolution of the South Pacific glacial carbon pool, Nature Communications, 7, 11 487, doi: 10.1038/ncomms11 487, 2016.

Rubino, M., Etheridge, D., Trudinger, C., Allison, C., Battle, M., Langenfelds, R., Steele, L., Curran, M., Bender, M., White, J., Jenk, T., Blunier, T., and Francey, R.: A revised 1000 year atmospheric δ^{13}C-CO_2 record from Law Dome and South Pole, Antarctica, Journal of Geophysical Research, 118, 8482–8499, 2013.

Sano, Y. and Williams, S. N.: Fluxes of mantle and subducted carbon along convergent plate boundaries, Geophysical Research Letters, 23, 2749–2752, 1996.

Schmitt, J., Schneider, R., Elsig, J., Leuenberger, D., Lourantou, A., Chappellaz, J., Köhler, P., Joos, F., Stocker, T., Leuenberger, M., and Fischer, H.: Carbon Isotope Constraints on the Deglacial CO_2 Rise from Ice Cores, Science, 336, 711–714, 2012.

Schmittner, A., Gruber, N., Mix, A. C., Key, R. M., Tagliabue, A., and Westberry, T. K.: Biology and air-sea gas exchange controls on the distribution of carbon isotope ratios in the ocean, Biogeosciences, 10, 5793–5816, 2013.

Schneider, R., Schmitt, J., Kohler, P., Joos, F., and Fischer, H.: A reconstruction of atmospheric carbon dioxide and its stable carbon isotopic composition from the penultimate glacial maximum to the last glacial inception, Climate of the Past, 9, 2507–2523, 2013.

Sikes, E., Cook, M., and Guilderson, T.: Reduced deep ocean ventilation in the Southern Pacific Ocean during the last glaciation persisted into the deglaciation, Earth and Planetary Science Letters, 438, 130–138, 2016.

Skinner, L. and Shackleton, N. J.: Rapid transient changes in northeast Atlantic deep water ventilation age across Termination I, Paleoceanography, 19, PA2005, doi:10.1029/2003PA000 983, 2004.

Skinner, L., McCave, I., Carter, L., Fallon, S., Scrivner, A., and Primeau, F.: Reduced ventilation and enhanced magnitude of the deep Pacific carbon pool during the last glacial period, Earth and Planetary Science Letters, 411, 45–52, 2015.

Skinner, L., Primeau, F., Freeman, E., de la Fuente, M., Goodwin, P. A., Gottschalk, J., Huang, E., McCave, I. N., Noble, T. L., and Scrivner, A. E.: Radiocarbon constraints on the glacial ocean circulation and its impact on atmospheric CO_2, Nature Communications, 8, 16 010, doi:10.1038/ncomms16 010, 2017.

Skinner, L. C., Fallon, S., Waelbroeck, C., Michel, E., and Barker, S.: Ventilation of the Deep Southern Ocean and Deglacial CO_2 Rise, Science, 328, 1147–1151, 2010.

Toggweiler, J. and Sarmiento, J.: Glacial to interglacial changes in atmospheric carbon dioxide: The critical role of ocean surface water in high latitudes, in The Carbon Cycle and Atmospheric CO_2: Natural Variations Archean to Present, Geophysical Monograph Series, American Geophysical Union, 32, 163–184, 1985.

Toggweiler, J. R.: Origin of the 100,000-year time scale in Antarctic temperatures and atmospheric CO_2, Paleoceanography, 23, PA2211, doi:10.1029/2006PA001 405, 2008.

Wolff, E., Barbante, C., Becagli, S., Bigler, M., Boutron, C., Castellano, E., de Angelis, M., Federer, U., Fischer, H., Fundel, F., Hansson, M., Hutterli, M., Jonsell, U., Karlin, T., Kaufmann, P., Lambert, F., Littot, G., Mulvaney, R., Roöthlisberger, R., Ruth, U., Severi, M., Siggaard-Andersen, M., Sime, L., Steffensen, J., Stocker, T., Traversi, R., Twarloh, B., Udisti, R., Wagenbach, D., and Wegner, A.: Changes in environment over the last 800,000 years from chemical analysis of the EPICA Dome C ice core, Quaternary Science Reviews, 29, 285–95, 2010.

Yu, J., Broecker, W., Elderfield, H., Jin, Z., McManus, J., and Zhang, F.: Loss of Carbon from the Deep Sea Since the Last Glacial Maximum, Science, 330, 1084–1087, 2010.

Yu, J., Anderson, R., Jin, Z., Rae, J., Opdyke, B., and Eggins, S.: Responses of the deep ocean carbonate system to carbon reorganization during the Last Glacial-interglacial cycle, Quaternary Science Reviews, 76, 39–52, 2013.

Yu, J., Anderson, R., Z.Jin, Menviel, L., Zhang, F., Ryerson, F., and Rohling, E.: Deep South Atlantic carbonate chemistry and increased interocean deep water exchange during last deglaciation, Quaternary Science Reviews, 90, 80–89, 2014a.

Yu, J., Anderson, R. F., and Rohling, E. J.: Deep ocean carbonate chemistry and glacial-interglacial atmospheric CO_2 changes, Oceanography, 27, 16–25, 2014b.

Yu, J., Menviel, L., Jin, Z. D., Thornalley, D., Barker, S., Marino, G., Rohling, E. J., Cai, Y., Zhang, F., Wang, X., Dai, Y., Chen, P., and Broecker, W. S.: Sequestration of carbon in the deep Atlantic during the last glaciation, Nature Geoscience, 9, 319–325, 2016.

Zeebe, R.: OSCAR: Long-term Ocean-atmosphere-Sediment Carbon cycle Reservoir Model v2.0.4, Geosci. Model Dev., 5, 149–166, 2012.

Zhao, N., Marchal, O., Keigwin, L., Amrhein, D., and Gebbie, G.: A Synthesis of Deglacial Deep-Sea Radiocarbon Records and Their (In)Consistency With Modern Ocean Ventilation, Paleoceanography and Paleoclimatology, 33, 128–151, 2017.